

Phase transition in vanadium oxide films formed by multistep deposition

V.P. Kladko, V.P. Melnik, O.I. Liubchenko, B.M. Romanyuk, O.Yo. Gudymenko, T.M. Sabov, O.V. Dubikovskiy, Z.V. Maksimenko, O.V. Kosulya, O.A. Kulbachynskiy, P.M. Lytvyn, O.O. Efremov

V. Lashkaryov Institute of Semiconductor Physics, National Academy of Sciences of Ukraine
41, prosp. Nauky, 03680 Kyiv, Ukraine
E-mail: kladko@isp.kiev.ua

Abstract. VO_x films deposited using the multistep method have been investigated. These films were prepared by repeating the two-stage method of low-temperature deposition and low-temperature annealing. The structure and characteristics of VO_x thin films have been studied. Taking into account the obtained results, theoretical modeling of the structure was performed and the parameters of the metal-insulator transition have been calculated.

Keywords: vanadium oxide films, phase transition, low-temperature annealing, theoretical modeling.

<https://doi.org/10.15407/spqeo24.04.362>

PACS 61.05.cp, 64.75.St, 68.55.-a, 73.61.-r, 81.15.Aa, 81.15.-z

Manuscript received 14.09.21; revised version received 08.10.21; accepted for publication 10.11.21; published online 23.11.21.

1. Introduction

Investigation of the physical properties of highly correlated systems is one of the most difficult subjects in physics of condensed matter, which generates controversial theoretical and experimental questions. Correlated vanadium-oxygen system with a wide variety of compounds, namely: VO, V₂O₃, V₂O₅, etc., and, especially, VO₂, is one of the most attractive functional materials [1–9]. This system is characterized by a phase transition (PT) from metal to insulator (MIT) with abrupt changes in optical, electrical, thermal and magnetic properties [3–8]. Formation of a large number of compounds in the vanadium-oxygen system [10, 11] leads to ambiguity of their electrophysical parameters. Vanadium dioxide (VO₂) is the most interesting compound in the V–O system, because PT in it takes place near the room temperature [12].

Although the mechanism of electrical and structural phase transition of VO₂ is still controversial, investigation and application of this effect have made significant progress in recent years for new electronic and photonic devices such as thermochromic “smart” glasses [13–15], microbolometers, etc.

The main problem in the synthesis process of vanadium-based films is simultaneous formation of different vanadium oxides (VO, V₂O₃, V₂O₅), as well as magnetic phases, namely: V₄O₉, V₆O₁₃, etc. Growing the stoichiometric VO₂ films requires precision control of

growth parameters during the process [16]. In practice, it is observed different defects, non-stoichiometry of surface layers and grain boundaries in VO₂ films and, as a consequence, the instability of their optical and electrical parameters [17, 18]. One of low cost growing methods of vanadium oxide films is magnetron sputtering. Using this method, polycrystalline VO₂ layers are synthesized at typical substrate temperature about 400...500 °C. For obtaining high-quality layers, the precision control of technological parameters, for example, base pressure of Ar and O₂ gases, is required. For these films, phase transition is observed without additional thermal annealing [19, 20]. If the substrate temperature is lower than 400 °C, good functionality of material from the viewpoint of PT cannot be obtained. Only further thermal annealing leads to the appearance of attractive film properties [21, 22].

In the papers [23–25], the two-stage method for low-temperature synthesis of VO_x layers was proposed: 1) magnetron sputtering of V target at the substrate temperature 200 °C and 2) subsequent thermal annealing of these films. Depending on the conditions of sputtering and annealing, it is possible to obtain either highly efficient thermochromic coatings or films with high temperature coefficient of resistance (TCR). This method works well for thin 100...200-nm films but with increasing of the layers' thickness, the electrical parameters deteriorate, and there are problems with films adhesion.

For microbolometric applications, the problem of lowering the PT temperature for films and increasing TCR remains relevant. Most of the proposed methods (introduction of impurities W [26], P, As, Bi [27], oxygen implantation [28, 29] decreases the temperature of PT, but this simultaneously decreases the changes in resistivity and optical transmittance, too. There is also a strong correlation between the width of the hysteresis loop and the size of VO₂ grains in the vanadium oxide systems. Recently, it has been shown that ensembles of nanometer particles have a wide hysteresis loop of phase transition during cyclic measurements [30]. Thus, it is emphasized that not only the component composition but also the size of crystallites and the stresses in them cause a strong effect on PT. Obviously, electrical changes in VO₂ films are an evidence of current transport through grain boundaries. The increase in the temperature resistance during thermal cycling corresponds to the increased resistance in the percolation systems that have the dominance of grain boundaries due to reduction grain sizes.

In this work, multilayered structures synthesized using two-stage growing method (magnetron sputtering at the substrate $T \sim 235$ °C and subsequent thermal annealing) were investigated. It is shown evolution of thin VO₂ films structural and electrical parameters during step-by-step formation. The mechanism of metal-insulator transition in VO₂ films was investigated.

2. Experimental

VO₂ thin films were grown on commercial Si (111) substrates by magnetron sputtering of VO₂ target. Before thin film deposition, the chamber was evacuated to a background pressure of $(1...2) \cdot 10^{-5}$ Torr. During the sputtering process, the Ar (high purity 99.999%) pressure was kept at $(2...4) \cdot 10^{-3}$ Torr. The power of magnetron was kept at 50...70 W, and substrate temperature was 235 ± 15 °C. After deposition, the samples were annealed at 350 °C for 30 min in Ar ambient.

The technological parameters of samples under investigation are shown in Table 1. The numbering of the sample $n(n-1)$ means that the technological procedure was performed on the sample $n-1$, *i.e.* the sample 6(5) passed three successive stages of sputtering and annealing. The sample 7 served as reference one, when a thick film was formed in one stage of sputtering and annealing.

Table 1. Technological parameters of film deposition.

Sample	Deposition time, min	Layer thickness, nm	Annealing
1	10	136	
2 (1)		135	+
3 (2)	15	370	
4 (3)		361	+
5 (4)	15	576	
6 (5)		570	+
7	40	595	
8(7)		580	+

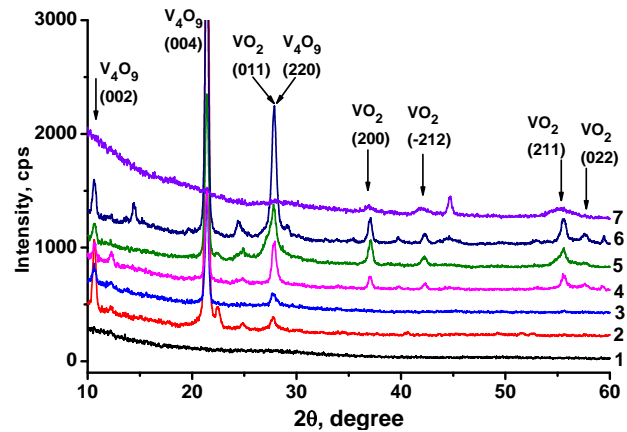


Fig. 1. X-ray diffraction patterns of the samples 1 to 7.

The crystal structure and structure-phase transitions (SPT) of the films were investigated using an X'Pert ProMPD X-ray diffractometer with the CuK_α wavelength ($\lambda = 0.15418$ nm). The film thickness was determined using a profilometer.

The surface nanorelief of annealed vanadium dioxide films was studied using atomic force microscopy (AFM) with a scanning probe microscope NanoScope IIIa Dimension 3000TM. Measurements were performed in the tapping mode by using the ultrasharp silicon probes with the nominal tip radius of 8 nm.

The resistances and TCR values of the films were measured using a two-point probe system with a heating unit within the range 25 °C to 90 °C.

3. Results and discussion

In Fig. 1, diffraction patterns of the samples 1–7 are shown. After depositing the first layer, the film has an amorphous structure, as evidenced by the presence of a halo in the region of the 2θ angle near 28 angle degrees (curve 1). Subsequent annealing leads to partial crystallization of the samples (curve 2). The dominant crystalline phase is V₄O₉ – 97% and VO₂(M) – 3%. After deposition of the following VO₂ layer, crystallinity of film decreases (curve 3). Formed two layers also contain an amorphous phase. The following annealing leads to a further increase in crystallinity of this film (curve 4). The intensity of existing peaks increases (reflection 001 of the VO₂ phase) and other reflections that belong to the monoclinic phase of VO₂ appear. The content of phase VO₂ is 42%, and V₄O₉ – 58%. Deposition of the next 3-rd layer almost do not effect on structure crystallinity (curve 5) in contrast to sputtering the second layer (sample 3).

Further annealing of this structure leads to better crystallization, as evidenced by an increase in the intensity of reflections and their half-widths (curve 6). The content of crystalline phase VO₂ in the samples 5 and 6 is close to 40%, and the content of the phase V₄O₉ is 60%. The diffraction pattern from the sample 8(7) (annealed thick layer) shows a weak crystallization

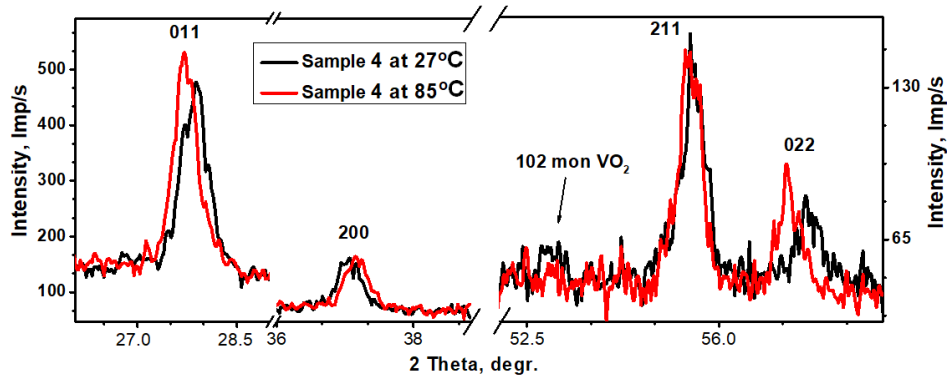


Fig. 2. Fragments of diffraction pattern from the sample 4 at different temperatures: before SPT – at 27 °C (black curve) and after SPT – at 85 °C (red curve). The main changes are shown for different angular intervals. (Color online.)

(Fig. 1, curve 7) after annealing. Predominantly the V_2O_3 and VO_2 phases begin to crystallize. Because this sample contained a small amount of VO_2 phase, there was no structural transition or metal-insulator transition; therefore, the sample 8 was not studied further.

Moreover, there is bad adhesion of film to substrate in the annealed sample 8, which is due to different thermal expansion coefficients in the layer and substrate. The small strain changes during formation of multilayer structure are observed in Fig. 1 as peak position shift. The most intensive peak 004 from V_4O_9 has angle position 21.427° and 21.43° for the samples 2 and 3, respectively. After annealing (sample 4), this peak position shifts to 21.413° , which indicates that strain state in film changes. After subsequent deposition and annealing (samples 5 and 6), peak position almost don't changes and are 21.418° and 21.408° for the samples 5 and 6, respectively. Thus, the method of sequential sputtering-annealing allows us to obtain thick layers through relaxation of strains at each deposition process, especially when overall structure thickness is small.

In Fig. 2, the structural-phase transition in the sample 4 was shown. Two diffraction patterns were measured: at room temperature and after heating up to 85 °C. It is observed peaks position shifts and intensity changes due to structural transformation from monoclinic structure to the tetragonal one. SPT occurs completely.

AFM measurements show that the surface of the films is an array of tightly packed grains of nanometer and sub-micrometer sizes (Fig. 3). At the micrometer level, the characteristic inhomogeneities caused by relaxation processes in films at annealing are shown. Thus, in the sample 2 there is a network of microcracks (Fig. 3a), in the vicinity of which the film is likely to peel off from the substrate and rises above the general level of the surface to the height approximately 4...8 nm (Fig. 4, curve a). Microcracks are distinguished by cells (blocks) of arbitrary shape with transverse dimensions of the order of 2...6 μm .

The samples 4 and 6 show a two-layer structure of the film, where there are recesses in the upper layers

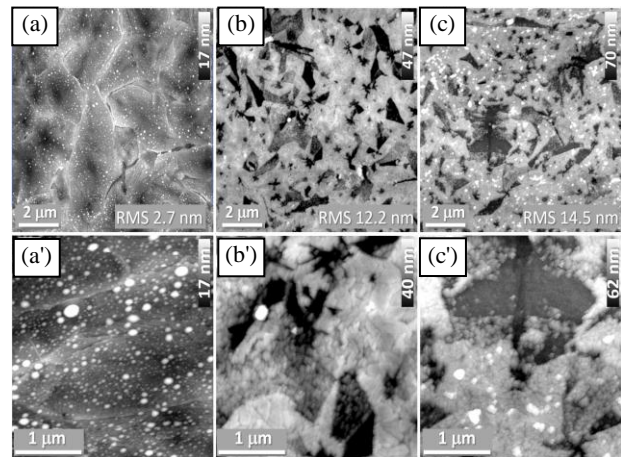


Fig. 3. AFM top-view of surfaces for the samples 2, 4, 6, (a, a'), (b, b'), (c, c'), respectively. Scanning field is 10×10 and $3 \times 3 \mu\text{m}$. Values of mean square roughness RMS of the surface are given in the figures.

(dark polygons in Figs 3b and 3c). The bottom of these recesses is flat, and the depth is close to 45...40 and 35...40 nm for the samples 4 and 6, respectively (Fig. 4, curves b, c). The transverse dimensions of the recesses vary from a few hundred nanometers to two micrometers. It can be assumed that the recesses are formed in the upper layers of the sputtered VO_2 film and their depth corresponds to the thickness of the upper layers.

It should be noted that in addition to recesses with the depths 35...50 nm, on films 4, 6 (especially 4) there are also recesses of the same planar configuration, but up to 10 nm deeper (lighter polygons in Fig. 3b).

The results of the analysis of annealed VO_2 films fine structure are shown in Fig. 5. The sample 2 is characterized by the presence of a bimodal granular structure. Dispersed grains with the sizes 30...100 nm cover the substrate that consists of the tightly-packed ones with the sizes 12...30 nm (Fig. 5a and box-diagram at the bottom of this figure).

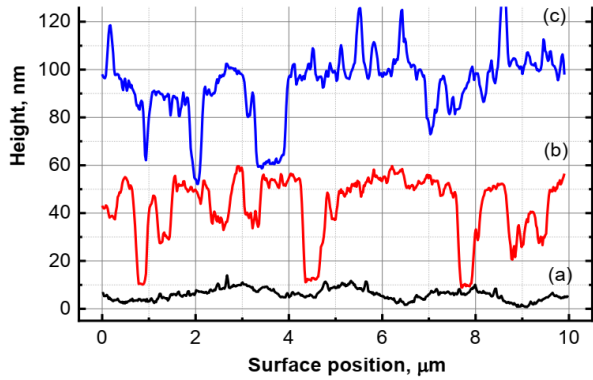


Fig. 4. Typical surface profile of the samples 2 (a), 4 (b) and 6 (c). Curves are shifted along the vertical direction for a better visualization.

These grains make up to 50% of the most common grains on the diagram as marked by the corresponding rectangular. The sample 6 has similar surface granularity, although the predominant quantity of grains has the sizes of 26 to 60 nm, and there are individual grains up to 150 nm.

In the sample 4, the most common size of grains is 40...70 nm; however, simultaneously there are grains with significantly larger sizes, mostly in the upper layer of the film. The transverse dimensions of these grains can reach 500 nm.

The power spectral density distribution (PSD) functions used for correlation analysis of surface heights, and the corresponding planar frequency characteristics of the relief elements (horizontal dimensions) are shown in Fig. 6.

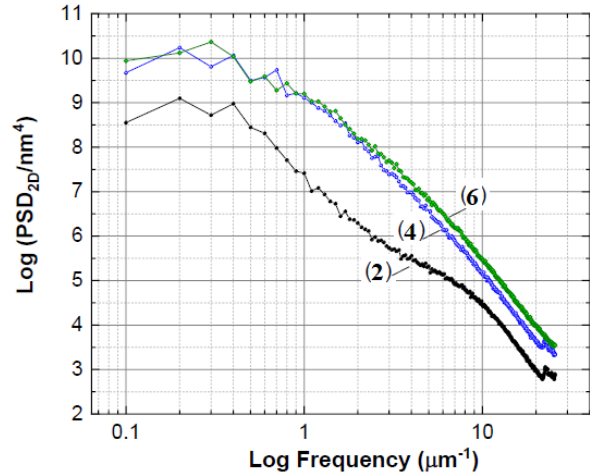


Fig. 6. Power spectral density of the relief spatial frequencies for the studied samples 2, 4 and 6.

In general, the low frequency plateau is characterized by aperiodic relief details and overall roughness. The roughness of the samples 4, 6 is an order of magnitude higher than the roughness of the sample 2 (RMS are 2.7, 12.2 and 14.4, respectively, for the samples 2, 4 and 6). In this case, the effective area of the surface is larger than that of the corresponding projection by 0.3% for the sample 2; 2.1% and 3.8% for the samples 4 and 6.

The inflection point (plateau completion) characterizes the correlation length of the relief elements, which for the sample 2 is close to 400 nm and about 220 nm for the samples 4 and 6.

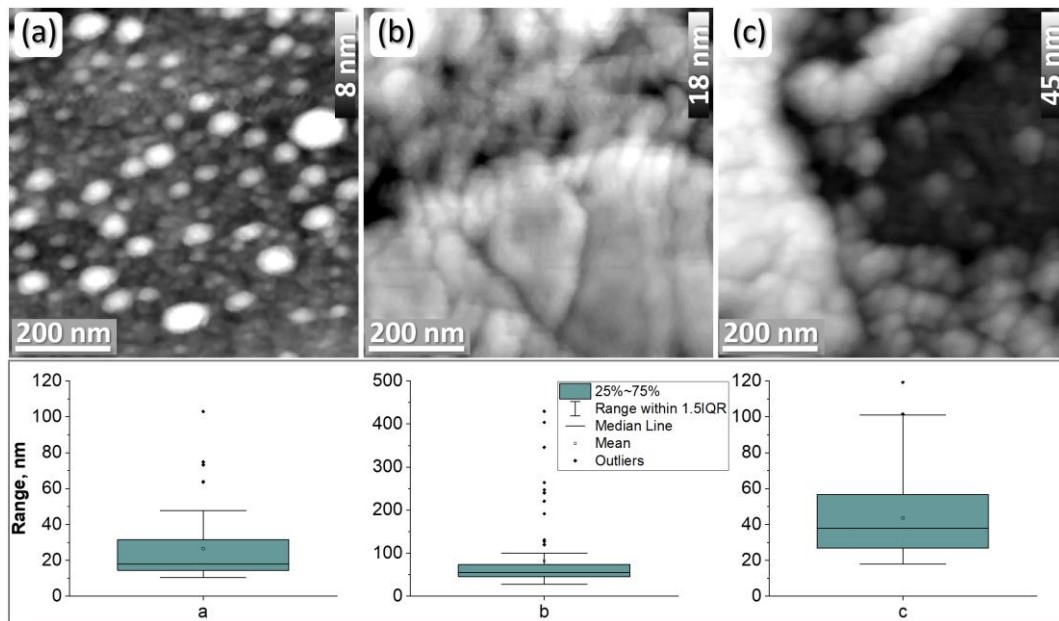


Fig. 5. Magnified AFM top-view of the samples 2, 4 and 6 surfaces, which are shown in Fig. 4, and box-diagrams of grains sizes, respectively.

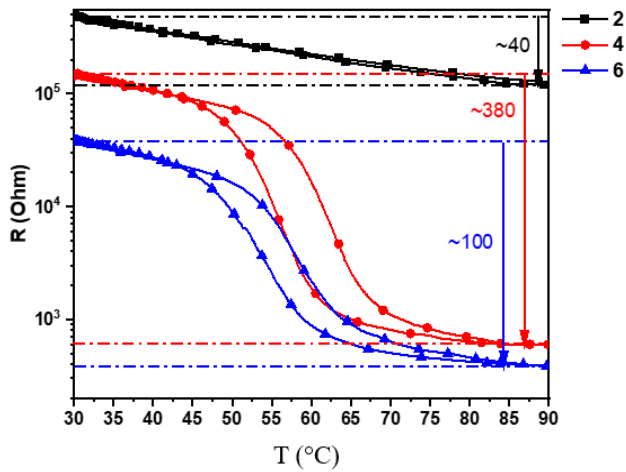


Fig. 7. Resistance dependence on temperature of vanadium oxide films deposited at $T_s = 235 \pm 15$ °C and annealed at 350 °C in Ar for 30 min for the samples 2, 4 and 6.

The slope of the curves in the high-frequency region characterizes the long-range correlation between the elements of the relief. For the samples 4 and 6, the slope is close (with a slightly better correlation for the sample 4). For the sample 2, there are two correlation dependences (two areas with different slopes). For relief elements from 400 down to 23 nm, the slope is much smaller, and the height of these surface relief elements is significantly smaller than in the samples 4, 6.

The correlation dependences of the surface elements less than 20 nm are similar to those in the samples 4, 6 with lower amplitude characteristics of the heights.

The temperature dependences of resistance during heating/cooling for the samples 2, 4 and 6 are shown in Fig. 7. The sharp metal-insulator transition (MIT) in the temperature range 50...60 °C is observed (Fig. 7). At the same time, the resistivity of the films decreases by almost two orders. Data on the values of the resistivity of the films before and after the phase transition are given in Table 2.

Table 2. Resistance before and after MIT.

Sample	Resistance at 30 °C (Ohm)	Resistance at 90 °C (Ohm)	ΔR , times
1	11 490	2 250	5.1
2	468 000	115 000	4.06
3	111 000	31 000	3.58
4	145 800	600	243
5	Initial resistance ~300 000 Ohm		
6	75 600	534	141
7	Initial resistance ~750 000 Ohm		
8	Initial resistance 500–700 Ohm		

The temperature change rate was 0.5 °C/s. When the speed decreases to 0.025 °C/s, the width of the hysteresis in the MIT region increases, namely, the location of the heating branches changes. The cooling branch does not change significantly. This effect needs to be further investigated.

The largest change in resistance by two orders of magnitude is observed in the samples 4 and 6. The hysteresis loop is located within the range from 40 up to 80 °C, the width of the hysteresis loop is $\Delta T \approx 1...10$ °C. The analysis of the MIT parameters was performed according to the nature of the first derivative dependence of the resistivity on temperature during the heating-cooling cycles for the samples deposited on the substrate after additional annealing in argon (350 °C, 30 min). According to the method described in [19], the maximum of the derivative corresponds to the transition temperature, the FWHM of the peak characterizes the transition speed, and the area under the curve characterizes the transition intensity (*i.e.*, shows how many orders of magnitude the film resistance decreases).

Considering sufficiently large value of FWHM, it is difficult to state unambiguously that there is a correlation between this value and the size of the crystallites. It is possible that during annealing two processes occur: oxidation of small crystallites and formation of additional crystallites due to crystallization of amorphous inclusions. For a more detailed study of physical processes in VO₂ film during thermal annealing, its elemental composition must be analyzed.

In Fig. 8, the dependence of temperature coefficient of resistance (TCR) from the temperature in the scale log(|TCR|) for the samples: 2 – black curve, 4 – red curve, 6 – blue curve are shown. Mark **H** – heating curve (solid line), **C** – cooling curve of the sample (dashed line).

As can be seen from the figure in the case of the sample 2, there is no extremum on the curves, which indicates the absence of MIT. For the samples 4 and 6 on the heating curves (**4H** and **6H**) there are maximums of TCR at 62.5 and 58.1 °C, respectively, which indicates the temperature of MIT. The temperature of MIT during cooling is 55.1 °C (**4C**) and 54.3 °C (**6C**). The hysteresis was 7.4 °C and 3.8 °C, respectively. Thereof, we can conclude that the deposition of the second layer leads to formation of a structure with a high content of VO₂ phase. The deposition of the third layer leads to a decrease in the hysteresis and temperature of MIT, but it also decreases the value of resistance change. This is related with formation of more homogeneous crystallites of the VO₂ phase in the film and an increase in tensile stresses. The decrease in the magnitude of resistance change, as well as the decrease in the resistance of the film at room temperature may be associated with formation of conductive phases of vanadium oxide.

In addition to estimating the parameters of the phase transition, namely TCR, numerical simulations of resistivity changes were performed. As the analysis of the experimental results shows, the resistance on both sides of MIT varies according to the exponential dependence of $R(T)$ (Figs 7 and 9). The insulating state often shows activated transport, $R \propto \exp(E/2k_B T)$.

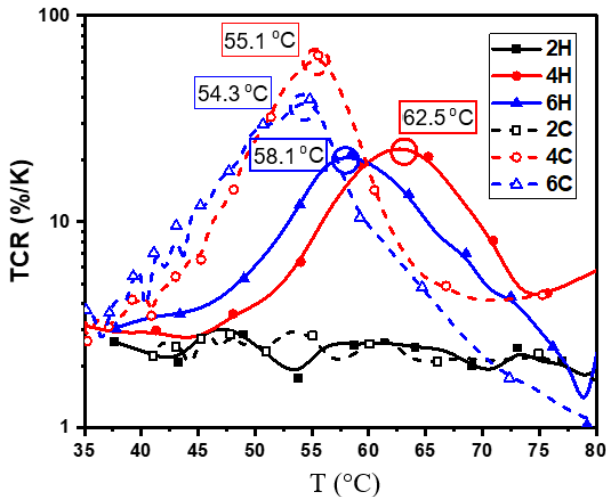


Fig. 8. Dependence of TCR from temperature.

The peculiarity of this behavior $R(T)$ in the samples has already been observed in [31], where the hypothesis about the absence of truly metallic state was proposed. Besides, as shown in the paper [32], annealing of different duration (0...1000 s) of deposited VO_2 films on the r - and a -plane sapphire in air ambient leads to a decrease in the change of $R(T)$ near MIT. The exponential dependence of $R(T)$ appears on the metal side (at the temperature higher than the MIT one). Longer annealing leads to the disappearance of the phase transition (like that in our sample 2 (Fig. 7)).

The main reason for this change of $R(T)$ is oxidation of VO_2 and accumulation of other phases (including dielectric V_2O_5) at the intergranular boundaries in the film [32]. Thus, the presence in the films of some variable amount of dielectric phase inactive from the viewpoint of MIT (like to that in V_2O_5) is the main reason for the observed phenomena, as it follows from this paper and the works [31, 32], moreover, the appearance of this phase is closely related to the introduction of additional oxygen into the sample. XRD analysis of our samples showed that this phase corresponds to V_4O_9 known from the literature [33]. Although V_4O_9 stoichiometrically close to monoclinic VO_2 , excess oxygen ($9/4 = 2.25$) leads to the appearance of a wide range of various near- and middle-ordered atomic configurations [34].

One of the goals of this simulation was to check the influence of residual dielectric phase (for example, V_4O_9 or V_2O_5) that can impose (at least partially) its $R(T)$ dependence to the metal side of MIT in VO_2 film. Another aim was to test how the structural imperfection of the metal phase can be revealed from the nature of the $R(T)$ curve.

In modeling, three types of film morphology were considered: 1) dielectric insulated metal grains, 2) random mixture of both phases with interpenetration and 3) dielectric grains in a metal frame. For the cases (1) and (3), the Odelevskii model was used for simulation [35–37], for the case (2) – effective environment model [36, 37].

When a random mixture of both phases with interpenetration is present, the residual dielectric inside the metal phase is actively shunted by the latter and cannot impose its activation temperature dependence on $R(T)$ on metal side of MIT. However, if the resistance difference for MIT is only 2-3 orders of magnitude, the “bad” metal with high resistivity (~ 1 kOhm) is present, in which the mean free path of carrier is small, either because of the structural imperfection in the metal itself, or because of the strong localization of electrons, which is typical for this material (VO_2) [2, 38].

In the case of “good” metal with low resistivity (~ 1 Ohm), the resistance difference for MIT significantly depends on the fraction of the residual dielectric phase, if the dielectric phase is concentrated at the boundaries of metal inclusions. This resistance difference can noticeably decrease from five orders of magnitude to one order with an increase in the fraction of the residual dielectric phase to 25%. In this case, the slope of the temperature dependences $\log R(T)$ on both sides of MIT is the same, which is demonstrated in the paper [31]. For “average” and “bad” metal (with resistivity 0.5 and 1 kOhm, respectively), the resistance difference for MIT can be even greater than in the previous case. The slope of dependence $\log R(T)$ at the metal side of PT gradually decreases with an increasing in the proportion of the metal phase and in common case is different than slope at the insulator side of MIT.

For other type of film morphology structures, when the metal phase either randomly bends around dielectric inclusions or encloses them in a more or less regular frame, the resistance at the metal side of MIT is independent on the temperature, which is observed in most cases described in the literature for pure metal. Calculations also showed that the phase inactive with respect to PT can significantly reduce the amplitude of the hysteresis loop, which was observed in [33].

Fig. 9 shows the results of numerical simulation of $R(T)$ dependence (curve 3 (cooling), curve 4 (heating)) for the samples 4 (a) and 6 (b) and its comparison with experimental results (curve 1 (cooling), 2 (heating)), which is in good agreement.

The resistance dependences far from MIT were approximated by exponential function (lines 7, 8 in Fig. 9). Taking into account the multiplicity, randomness and (in the first approximation) the independence of temperatures of MIT in each crystallite, the distribution of local MIT temperatures was proposed to describe as the Gaussian distribution. This distribution of MIT temperature in the samples during phase transition was presented by curves 5, 6 in Fig. 9 – cooling and heating, respectively. For the sample 4, Gaussian was centered at 60 °C (cooling) and 65 °C (heating) with a deviation of temperature $\sigma_T = 10$ °C. To the left of MIT, the resistance changes exponentially (activation energy is 0.46 eV), to the right – it is almost constant. In the sample 4, the conductive phase is more pronounced like to metal.

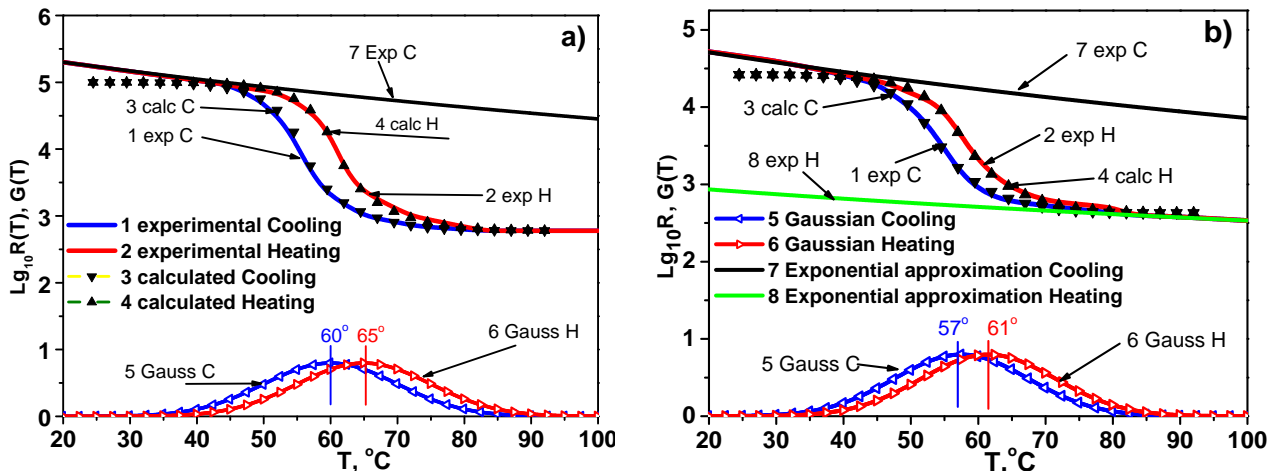


Fig. 9. Modeling of MIT for the samples 4 (a) and 6 (b).

The difference in resistance at MIT is 166 times. The heating-cooling hysteresis is approximately 5 °C. For the sample 6, T_{MIT} was centered at $T = 57$ °C (cooling) and 61 °C (heating). The deviation σ_T was 9...10 °C. For the sample 6, the heating-cooling hysteresis is close to 4 °C. The difference in resistance at the transition is 62 times. On both sides of the phase transition, the resistance changes exponentially. The effective activation energies are 0.493 and 0.307 eV. A slight lag of the calculated data from the experimental at $T = 40$ °C indicates percolation effects, when the experimental conductivity increases earlier than the calculated one due to the appearance of an infinite cluster. The values of hysteresis 5 °C and 4 °C obtained from simulation are close for experimental values 7.4 °C and 3.8 °C for the samples 4 and 6, respectively.

Hence, the simulation results show that, in our case, VO_2 crystallites enclosed in a thin dielectric framework V_4O_9 (exponential temperature dependence of resistance far from MIT) and are structurally disordered. As a result, due to disordering, the mean free path of electrons in such a metal is very small. After the phase transition, the metallic phase of VO_2 is a “bad” metal, since: 1) the resistance drop at the phase transition metal-insulator is close to two orders of magnitude, and 2) the effective activation energy from the dependence $R(T)$ on the metal side of MIT is half or more times less than on the dielectric side. Structural disorder is more pronounced in the 3-layer sample 6, because, as mentioned above, in the sample 4 the high-temperature phase is an “average” metal.

Based on these phenomenological calculations, it was obtained the criteria which made it possible, based only on the temperature dependence of the resistance, to judge the quality of the atomic structure of the metallic phase itself (value of structural disordering) and estimate type of the film morphology.

If the relief of the surface in the samples 4 and 6 (Figs 3b and 3c, respectively) is compared, then some similarities in the block structure of the films surface became obvious, therefore, the parameters of the

temperature hysteresis loops of the resistance are close. The main difference between the samples 4 and 6 textures is the presence of singular needle relief at the surface of sample 6. But the influence of this relief on MIT parameters is obviously negligible.

The simulation results indicate that the phase V_4O_9 , observed on XRD spectra concentrates at the grain boundaries and, most likely, on the film interfaces, where oxygen can accrue. However, according to AFM data, the sample 4 has a larger grain size than the sample 6. Due to larger grain sizes in the sample 4, the influence of grain boundaries on electrical parameters is sufficiently weaker than in the sample 6, which explains the better value of TCR and resistivity changes in the sample 4.

The method of sequential two-stage deposition of VO_x films is proposed. This method allows us to create thick (>500 nm) VO_x films with good adhesion, high content of VO_2 nanocrystallites and low content of other vanadium oxides phases. Simulation showed that the film consists of VO_2 crystallites enclosed in a thin dielectric framework V_4O_9 . The high value of TCR in these films makes them promising to be used as functional layers in uncooled microbolometers.

Acknowledgments

The present work was supported by the National research foundation of Ukraine (project No 2020.02/0054).

References

1. Goodenough J.B. Metallic oxides. *Prog. Solid State Chem.* 1971. **5**. P. 145–399. [https://doi.org/10.1016/0079-6786\(71\)90018-5](https://doi.org/10.1016/0079-6786(71)90018-5).
2. Dobrosavljevic V., Trivedi N., Valles J.M., Jr. *Conductor-Insulator Quantum Phase Transitions*. Published to Oxford Scholarship Online, 2012.
3. Liu K., Lee S., Yang S., Delaire O., Wu J. Recent progresses on physics and applications of vanadium dioxide. *Materials Today*. 2018. **21**, No 8. P. 875–896. <https://doi.org/10.1016/j.mattod.2018.03.029>.

4. Kasirga T., Sun D., Park J. *et al.* Photoresponse of a strongly correlated material determined by scanning photocurrent microscopy. *Nat. Nanotechnol.* 2012. **7**. P. 723–727. <https://doi.org/10.1038/nnano.2012.176>.
5. Liu K., C Ch., Cheng Z. *et al.* Giant-amplitude, high-work density microactuators with phase transition activated nanolayer bimorphs. *Nano Lett.* 2012. **12**, No 12. P. 6302–6308. <https://doi.org/10.1021/nl303405g>.
6. Bae S.-H., Lee S., Koo H. The memristive properties of a single VO₂ nanowire with switching controlled by self-heating. *Adv. Mater.* 2013. **25**, No 36. P. 5098–5103. <https://doi.org/10.1002/adma.201302511>.
7. Hu B., Ding Y., Chen W. *et al.* External-strain induced insulating phase transition in VO₂ nanobeam and its application as flexible strain sensor. *Adv. Mater.* 2010. **22**, No 45. P. 5134–5139. <https://doi.org/10.1002/adma.201002868>.
8. Savo S., Zhou Y., Castaldi G. *et al.* Reconfigurable anisotropy and functional transformations with VO₂-based metamaterial electric circuits. *Phys. Rev. B.* 2015. **91**, No 13. P. 134105. <https://doi.org/10.1103/PhysRevB.91.134105>.
9. Kats M.A., Blanchard R., Zhang S. *et al.* Vanadium dioxide as a natural disordered metamaterial: Perfect thermal emission and large broad-band negative differential thermal emittance. *Phys. Rev. X.* 2013. **3**, No 4. P. 041004. <https://doi.org/10.1103/PhysRevX.3.041004>.
10. Wriedt H.A. The O-V (Oxygen-Vanadium) system. *Bull. of Alloy Phase Diagrams.* 1989. **10**, No 3. P. 271–277. <https://doi.org/10.1007/BF02877512>.
11. D’Elia A., Rezvani S.J., Zema N. *et al.* Stoichiometry and disorder influence over electronic structure in nanostructured VO_x films. *J Nanopart Res.* 2021. **23**, No 1. Article: 33. <https://doi.org/10.1007/s11051-020-05130-z>.
12. Morin F. Oxides which show a metal-to-insulator transition at the Neel temperature. *Phys. Rev. Lett.* 1959. **3**, No 34. P. 34–36. <https://doi.org/10.1103/PhysRevLett.3.34>.
13. Blackman C.S., Piccirillo C., Binions R., Parkin I.P. Atmospheric pressure chemical vapour deposition of thermochromic tungsten doped vanadium dioxide thin films for use in architectural glazing. *Thin Solid Films.* 2009. **517**, No 16. P. 4565–4570. <https://doi.org/10.1016/j.tsf.2008.12.050>.
14. Warwick M., Binions R. Advances in thermochromic vanadium dioxide films. *J. Mater. Chem. A.* 2014. **2**. P. 3275–3292. <https://doi.org/10.1039/C3TA14124A>.
15. Gao Y., Luo H., Zhang Z. *et al.* Nanoceramic VO₂ thermochromic smart glass: A review on progress in solution processing. *Nano Energy.* 2012. **1**. P. 221–246. <https://doi.org/10.1016/j.nanoen.2011.12.002>.
16. Schlag H.J., Scherber W. New sputter process for VO₂ thin films and examination with MIS-elements and C–V-measurements. *Thin Solid Films.* 2000. **366**, No 1-2. P. 28–31. [https://doi.org/10.1016/S0040-6090\(00\)00711-2](https://doi.org/10.1016/S0040-6090(00)00711-2).
17. Wei J., Ji H., Guo W.H., Nevidomskyy A.H., Natelson D. Hydrogen stabilization of metallic vanadium dioxide in single-crystal nanobeams. *Nat. Nanotechnol.* 2012. **7**. P. 357–362. <https://doi.org/10.1038/nnano.2012.70>.
18. Wu C.Z., Wei H., Ning B., Xie Y. New vanadium oxide nanostructures: Controlled synthesis and their smart electrical switching properties. *Adv. Mater.* 2010. **22**, No 17. P. 1972–1976. <https://doi.org/10.1002/adma.200903890>.
19. Brassard D., Fourmax S., Jean-Jacques M., Kieffer J.C., El Khakani M.A. Grain size effect on the semiconductor-metal phase transition characteristics of magnetron-sputtered VO₂ thin films. *Appl. Phys. Lett.* 2005. **87**, No 5. P. 051910. <https://doi.org/10.1063/1.2001139>.
20. Bialas H., Dillenz A., Downar H., Ziemann P. Epitaxial relationships and electrical properties of vanadium oxide films on r-cut sapphire. *Thin Solid Films.* 1999. **338**, No 1-2. P. 60–69. [https://doi.org/10.1016/S0040-6090\(98\)00995-X](https://doi.org/10.1016/S0040-6090(98)00995-X).
21. Lee M.-H., Kim M.-G. RTA and stoichiometry effect on the thermochromism of VO₂ thin films. *Thin Solid Films.* 1996. **286**, No 1-2. P. 219–222. [https://doi.org/10.1016/S0040-6090\(96\)08536-7](https://doi.org/10.1016/S0040-6090(96)08536-7).
22. Lopez R., Feldman L.C., Haglund R.F. Size-dependent optical properties of VO₂ nanoparticle arrays. *Rev. Lett.* 2004. **93**, No 17. P. 177403. <https://doi.org/10.1103/PhysRevLett.93.177403>.
23. Goltvyanskyi Yu., Khatsevych I., Kuchuk A. *et al.* Structural transformation and functional properties of vanadium oxide films after low-temperature annealing. *Thin Solid Films.* 2014. **564**. P. 179–185. <https://doi.org/10.1016/j.tsf.2014.05.067>.
24. Melnyk V.P., Khazevich I.V., Kladko V.P., Kuchuk A.V., Nikirin V.V., Romanyuk B.M. Low-temperature method for thermochromic high ordered VO₂ phase formation. *Mater. Lett.* 2012. **68**. P. 215–217. <https://doi.org/10.1016/j.matlet.2011.10.075>.
25. Melnik V.P., Khatsevych I.M., Goltvyanskyi Yu.V. *et al.* Thermochromic properties of vanadium dioxide films obtained by magnetron sputtering. *Ukr. J. Phys.* 2011. **56**, No 6. P. 534–540.
26. Romanyuk A., Steiner R., Marot L., Oelhafen P. Temperature-induced metal–semiconductor transition in W-doped VO₂ films studied by photoelectron spectroscopy. *Solar Energy Materials & Solar Cells.* 2007. **91**, No 19. P. 1831–1835. <https://doi.org/10.1016/j.solmat.2007.06.013>.
27. Ren Q., Cai Y., Gao Y. DFT study of M-doped (M=P, As, Bi) VO₂ for thermochromic energy-saving materials. *Comput. Mater. Sci.* 2018. **150**. P. 337–345. <https://doi.org/10.1016/j.commatsci.2018.04.015>.
28. Heckman E.M., Gonzalez L.P., Guha S., Barnes J.O., Carpenter A. Electrical and optical switching properties of ion implanted VO₂ thin films. *Thin Solid Films.* 2009. **518**, No 1. P. 265–268. <https://doi.org/10.1016/j.tsf.2009.05.063>.

29. Sabov T.M., Oberemok O.S., Dubikovskiy O.V. *et al.* Oxygen ion-beam modification of vanadium oxide films for reaching a high value of the resistance temperature coefficient. *Semiconductor Physics, Quantum Electronics & Optoelectronics*. 2017. **20**, No 2. P. 153–158.
<https://doi.org/10.15407/spqeo20.02.153>.
30. Théry V., Boule A., Crunteanu A. *et al.* Role of thermal strain in the metal-insulator and structural phase transition of epitaxial VO₂ films. *Phys. Rev. B*. 2016. **93**, No 18. P. 184106.
<https://doi.org/10.1103/PhysRevB.93.184106>.
31. Mani R.G., Ramanathan S. Observation of a uniform temperature dependence in the electrical resistance across the structural phase transition in thin film vanadium oxide (VO₂). *Appl. Phys. Lett.* 2007. **91**, No 6. P. 062104.
<https://doi.org/10.1063/1.2767189>.
32. Dou Y.-K., Li J.-B., Cao M.-S. *et al.* Oxidizing annealing effects on VO₂ films with different microstructures. *Appl. Surf. Sci.* 2015. **345**. P. 232–237. <http://dx.doi.org/10.1016/j.apsusc.2015.03.044>.
33. Yamazaki S., Li Ch., Ohoyama K., Nishi M., Ichihara M., Ueda H., Ueda Y. Synthesis, structure and magnetic properties of V₄O₉ – A missing link in binary vanadium oxides. *J. Solid State Chem.* 2010. **183**, No 7. P. 1496–1503.
<https://doi.org/10.1016/j.jssc.2010.04.007>.
34. Elliott S.R. Medium-range structural order in covalent amorphous solids. *Nature*. 1991. **354**. P. 445–452. <https://doi.org/10.1038/354445a0>.
35. Odelevskii V.I. Calculation of generalized conductivity of heterogeneous systems. *Zhurnal Tekhnicheskoi Fiziki*. 1951. **21**. P. 1379–1381 (in Russian).
36. Dulnev G.N. and Zarichnyak Y.P. *Thermal Conductivity of Mixtures and Composite Materials*. Leningrad, Energy, 1974 (in Russian).
37. Dulnev G.N. and Novikov V.V. *Transport Processes in Inhomogeneous Media*. Leningrad, Energoatomizdat, 1991 (in Russian).
38. Bugaev A.A., Zaharchenia B.P., Chudnovskiy F.A. *Metal-Semiconductor Phase Transition and its Applications*. Leningrad, Nauka, 1979 (in Russian).

Authors and CV



Vasyl Kladko, Doctor of Sciences (Physics and Mathematics), Corresponding Member of the National Academy of Sciences of Ukraine, Head of the Department of Structural and Elemental Analysis of Materials and Systems at the V. Lashkaryov Institute of Semiconductor Physics.

Author of more than 300 publications. His research interests include: solid-state physics, dynamical theory of diffraction of radiation, X-ray optics, X-ray diffraction analysis of semiconductor crystals, hetero- and nanosystems. E-mail: kladko@isp.kiev.ua; <https://orcid.org/0000-0002-1531-4219>.



Victor Melnik, Doctor of Sciences (Physics and Mathematics), Senior Researcher at the Department of Ion-Beam Engineering, V. Lashkaryov Institute of Semiconductor Physics. Author of more than 150 scientific publications. His research interests include: solid-state physics, ion-beam material synthesis, SIMS spectroscopy.

E-mail: melnik@isp.kiev.ua;
<https://orcid.org/0000-0002-8670-7415>



Alexey Liubchenko graduated from the National Technical University of Ukraine “Igor Sikorsky Kyiv Polytechnic Institute” in 2015. PhD, Researcher at the Department for Diffraction Analysis of the Structure of Semiconductors, V. Lashkaryov Institute of Semiconductor Physics.

The area of scientific interests is analysis of materials science objects, high-resolution X-ray diffraction and computer simulation of XRD spectra. Authored 6 articles.

E-mail: Lubchenko.A@gmail.com;
<https://orcid.org/0000-0002-9773-0661>.



Boris Romanyuk, Doctor of Sciences (Physics and Mathematics), Chief Researcher at the Head of Department of Ion-Beam Engineering, V. Lashkaryov Institute of Semiconductor Physics. Author of more than 200 scientific publications, 20 patents for inventions. His research interests include: physics of

semiconductors and dielectrics, thanks to the landmark work to create the direction of ion-implant engineering and conducting a wide range of studies of semiconductor structures.

E-mail: romb@isp.kiev.ua;
<https://orcid.org/0000-0002-1688-7588>



Olexandr Gudymenko, PhD in Physics and Mathematics, Researcher at the Department of Structural and Elemental Analysis of Materials and Systems at the V. Lashkaryov Institute of Semiconductor Physics. Author of more than 56 publications. His research interests include: solid-state physics, dynamical theory of diffraction of radiation, X-ray optics,

X-ray diffraction analysis of semiconductor crystals, hetero- and nanosystems, XRD analysis of materials, X-ray reflectometry of thin films.

E-mail: gudymen@ukr.net;
<https://orcid.org/0000-0002-5866-8084>



Tomash Sabov, PhD in Physics and Mathematics, Junior Researcher at the Department of Ion Beam Engineering at the V. Lashkaryov Institute of Semiconductor Physics. He is the author of more than 20 publications. His main research activity is physics of thin films, chromogenic materials and SIMS analysis.

E-mail: Tsabov92@gmail.com;
<https://orcid.org/0000-0003-2636-2379>



Oleksandr Dubikovskiy, Junior Researcher at the Department of Ion-Beam Engineering at the V. Lashkaryov Institute of Semiconductor Physics. He is the author of more than 16 publications. The main directions of his scientific researches are studying the ion-beam modification processes and

mass spectrometric analysis of semiconductor structures.

E-mail: Dubikovsky_o@ukr.net;
<https://orcid.org/0000-0002-1504-8440>



Zoya Maksimenko, PhD in Physics and Mathematics, Researcher at the Department of Structural and Elemental Analysis of Materials and Systems at the V. Lashkaryov Institute of Semiconductor Physics. The main direction of her scientific activity is studying the semiconductor nanostructures by using high-resolution

X-ray diffractometry in the field of anomalous X-ray dispersion.

E-mail: ZMaksimenko@gmail.com;
<https://orcid.org/0000-0002-3434-3728>



Oleksandr Kosulya, PhD in Physics and Mathematics, Researcher at the Department of Ion-Beam Engineering, V. Lashkaryov Institute of Semiconductor Physics. His research interests include: secondary ion mass spectrometry, ion implantation, analysis of thin-film and multilayer structures, analysis of chemical composition. E-mail: Alexandr250990@gmail.com
<https://orcid.org/0000-0001-7642-8052>



Oleksandr Kulbachynskiy, Junior Researcher at the Department of Ion-Beam Engineering at the V. Lashkaryov Institute of Semiconductor Physics. His main research activity is physics of thin films, chromogenic materials and SIMS analysis, ion implantation, analysis of thin-film and multilayer structures.

E-mail: s.kulbachynskiy@gmail.com



Petro Lytvyn, PhD in Physics and Mathematics, Senior Researcher of Laboratory of Electron probe methods of structural and elemental analysis of semiconductor materials and systems at the V. Lashkaryov Institute of Semiconductor Physics. The area of scientific interests includes the AFM and X-ray investigations of semiconductor materials and systems.

E-mail: plyt2007@gmail.com;
<https://orcid.org/0000-0002-0131-9860>



Oleksiy Efremov, PhD in Physics and Mathematics, Senior Researcher of Laboratory of Electron probe methods of structural and elemental analysis of semiconductor materials and systems, V. Lashkaryov Institute of Semiconductor Physics.

E-mail: efremov@isp.kiev.ua;
<https://orcid.org/0000-0001-9608-6571>

Фазовий перехід у плівках оксиду ванадію, утворених багатоступеневим осадженням

В.П. Кладько, В.П. Мельник, О.І. Любченко, Б.М. Романюк, О.Й. Гудименко, Т.М. Сабов, О.В. Дубіковський, З.В. Максименко, О.В. Косуля, О.А. Кульбачинський, Р.М. Литвин, О.О. Єфремов

Анотація. Досліджено плівки VO_x , нанесені багатоступеневим методом. Ці плівки було отримано методом двоетапного низькотемпературного осадження з наступним низькотемпературним відпалом. Досліджено структуру та характеристики тонких плівок VO_x . З урахуванням отриманих результатів проведено теоретичне моделювання структури та розраховано параметри переходу метал-ізолятор.

Ключові слова: плівки оксиду ванадію, фазовий перехід, низькотемпературний відпал, теоретичне моделювання.